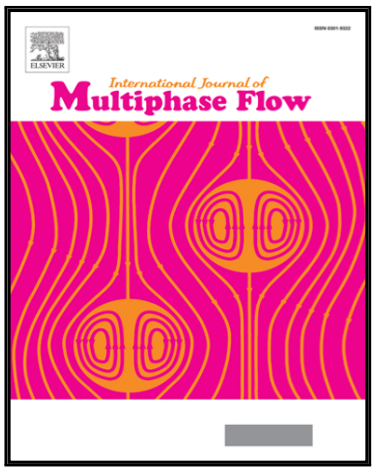

Flow characteristics in pressurized oxy-fuel fluidized bed under hot condition

Lin Li , Yuanqiang Duan , Lunbo Duan , Chuanlong Xu , Edward John Anthony

PII: S0301-9322(18)30241-6
DOI: 10.1016/j.ijmultiphaseflow.2018.06.020
Reference: IJMF 2848

To appear in: *International Journal of Multiphase Flow*

Received date: 7 April 2018
Revised date: 8 June 2018
Accepted date: 25 June 2018

Please cite this article as: Lin Li , Yuanqiang Duan , Lunbo Duan , Chuanlong Xu , Edward John Anthony , Flow characteristics in pressurized oxy-fuel fluidized bed under hot condition, *International Journal of Multiphase Flow* (2018), doi: 10.1016/j.ijmultiphaseflow.2018.06.020

Highlights

- The u_{mf} was measured in high pressure and high temperature;
- A formula for calculating the u_{mf} was established;
- Bubble characteristics were studied by visualized pressurized fluidized bed.

International Journal of Multiphase Flow, Volume 108, November 2018, Pages 1-10
DOI: 10.1016/j.ijmultiphaseflow.2018.06.020

Flow characteristics in pressurized oxy-fuel fluidized bed under hot condition

Abbreviated title: Flow characteristics of oxy-fuel PFB

Lin Li[1], Yuanqiang Duan[1], Lunbo Duan[1,*], Chuanlong Xu[1], Edward John Anthony[2]

1. Key Laboratory of Energy Thermal Conversion and Control, Ministry of Education, School of Energy and Environment, Southeast University, Nanjing 210096, China
2. Centre for Combustion and CCS, School of Energy, Environment and Agrifood, Cranfield University, Cranfield, Bedfordshire MK43 0AL, UK

*Corresponding author. Tel: +86 25 83790147; E-mail: duanlunbo@seu.edu.cn (L. Duan).

Co-author email address: lilin19901210@126.com (L. Li); 374321690@qq.com (Y. Duan); chuanlongxu@seu.edu.cn (C. Xu); b.j.anthony@cranfield.ac.uk (E. J. Anthony)

Abstract:

Pressurized oxy-fuel fluidized bed (POFB) combustion is regarded as a promising technology for carbon capture from coal-fired power plants. High pressure and temperature conditions have important impacts on the flow characteristic of fluidized bed, and understanding them will help to optimize the design and operation of the POFB boiler. In this work, experiments were carried out in two pressurized fluidized bed (PFB) devices (a hot PFB and a "visual PFB") both operated under high temperature (20-800 °C) and high pressure conditions (0.1-1.0 MPa). Four parameters including the minimum fluidization velocity (u_{mf}), the minimum bubbling velocity (u_{mb}), bubble diameter (D_b) and bubble frequency (f) were examined in this study. Results showed that the u_{mf} decreases with rising pressure and temperature. Based on our results

a formula was fitted for calculating the minimum fluidization velocity in PFB, with a relative error less than 15%. With the increase of fluidization number (*w*), the bubble size and tail vortex increased gradually, the bubbles tended to merge, and the shape of bubbles became more irregular. The D_b decreases with the increase of temperature and pressure at the same *w*. The *f* increases with increased *w*, while it decreased with the increase of temperature and pressure.
Keywords: *Fluidized Bed, high temperature, high pressure, the minimum fluidization velocity, bubble behaviour.*

1. Introduction

Coal has been and will continue to be one of the major energy sources in the foreseeable future due to its wide distribution, abundant reserves and competitively low price, especially for power generation (Buhre, et al., 2005; Shaddix, 2012). However, large amounts of CO_2 emitted from coal-fired power plants will cause a harmful impact on the global climate (Hansen et al., 1981). By allowing the capture of CO_2 from coal-fired power plants, oxy-fuel combustion technology is regarded as a promising near-zero emission technology. However, its higher economic costs and lower efficiency still limit its commercialization. In conventional oxy-fuel combustion system, the air separation unit (ASU) and the compression purification unit (CPU) function under high pressure, while the boiler runs at atmospheric pressure. This pressure differential causes energy losses and a reduction of net efficiency (Duan et al., 2017).

In recent years, pressurized oxy-fuel combustion (POFC) technology, representing

as it does a second generation oxy-fuel combustion technology; has aroused widespread interest in academia and industry. In 2012, in a GTI and CanmetENERGY cooperation, a $1MW_{th}$ pressurized fluidized bed oxygen-fuel combustion pilot project was funded by the US Department of Energy (DOE), and this is currently its largest funded project. In addition, the Italian IETA (Benelli et al., 2008), the Polish Institute for Chemical Processing of Coal (Lasek et al., 2012; Lasek et al., 2013) and several other research institutions (Lei et al., 2012) have carried out relevant research in this area. Since the whole system runs under high pressure, the energy loss caused by pressure fluctuation can be significantly reduced compared to atmospheric oxy-fuel combustion system. In addition, many other advantages can be gained by means of POFC technology (Duan et al., 2017; Li et al., 2013), these include: (1) Reducing the boiler size and equipment costs; (2) Recovering latent heat from flue gas; (3) Avoiding air leakage, thus ensuring a relatively low cost for CPU; (4) increasing the convective heat transfer for a given mean velocity; (5) reducing the cost of flue gas recirculation fan and the CPU system.

In the POFC technology, the pressurized boiler is the most important component, whose performance will be directly affected by the overall efficiency of the entire system. Up to now, the most mature aspect of this technology is the pressurized fluidized bed (PFB), which has been widely-used in the chemical industry. In addition, employing PFB technology in oxy-fuel combustion has numerous advantages including increased range of fuel types, flexible furnace temperature control by solid recycle, as well as inherently low SO_2 and NO_x emissions.

The most basic characteristics, the flow characteristics (including the minimum fluidization velocity, bubbling characteristics, etc.) have a crucial impact on gas-solid mixing, heat transfer, mass transfer and chemical reactions in pressurized fluidized bed (PFB) boilers (Jin et al., 1991). Therefore, this has been the main focus of research up to now.

Douglas et al. (1984) studied the minimum fluidization velocity (u_{mf}) of particles at different pressure, and concluded that the u_{mf} decreased as the pressure increase for the larger particles and the u_{mf} had no connection with pressure for small particles. Similar conclusions can be found elsewhere (Li et al., 2013; King et al., 1982; Sidorenko et al., 2004; Sobreiro et al., 1982). However, all of these studies were carried out at low temperatures. Saxena (1977) studied the fluidization characteristics of dolomite particles and concluded that the u_{mf} was less affected by temperature. Similar conclusions were also obtained by Girimonte et al. (2009) and Formisani et al. (1998). By contrast, Goo et al. (2009) and Subramani et al. (2007) argued that u_{mf} decreased with the increasing

temperature at lower temperature ranges, but that it was almost constant at high temperatures. Ma et al. (2013) measured the u_{mf} of quartz sand particles with particle diameter of 0.5 mm and 1.3 mm in 30-600 °C and concluded that the u_{mf} reduced as the temperature increased. It is evident that disagreements on the effect of temperature on u_{mf} still exists and needs to be further studied.

Since image processing technology can determine the flow characteristics in real time without interfering with the original flow field, many researchers have adopted this method to study bubble behavior in fluidized bed. Antonio et al. (2008) measured the bubble size, bubble velocity and bed voidage by digital image analysis and compared them with the theoretical results. Movahedirad et al. (2012) studied the characteristics of bubble behavior on a two-dimensional bubbling fluidized bed by means of experiment and simulation, and the simulation results agreed well with the experimental results. Caicedo et al. (2003) investigated the effects of different operating conditions on the shape factor and aspect ratio by using the image processing method, and verified the importance of CCD camera and further elucidated the behavior of the 2D fluidized bed. Shen et al. (2004) studied bubble size and bubble velocity in a two-dimensional cold fluidized bed using a visualization technique and found that bubble size increased with the increment of the fluidization number (w) and the height above air distributor.

Because of the difficulty in design and operation of hot PFB reactors, existing research has mainly focused on the effect of either room temperature or atmospheric pressure, which differs significantly from the real combustion state (high temperature

and pressure) of the PFB boiler in terms of gas parameters, bed resistance and bubble behavior. Therefore, the flow characteristics of PFB at high temperature and pressure needs to be systematically studied.

The goal of the present work is to investigate the flow characteristics (minimum fluidized velocity, minimum bubbling velocity, bubble size and frequency, etc.) of pressurized fluidized bed under different operating conditions (temperature, pressure and bed material). The experiments were performed separately in two experimental devices. The u_{mf} was obtained by monitoring bed pressure drop in a hot pressurized fluidized bed. The bubbling behavior was recorded by a high-speed CCD camera in the visualized pressurized bubbling fluidized bed.

2. Experimental

2.1 Experimental Apparatus

2.1.1 Hot pressurized fluidized bed

The schematic diagram of the hot pressurized fluidized bed system is shown in Fig. 1. The experimental system consisted of a fluidized bed reactor, preheating section, a temperature controlling system, a pressure measuring system, a gas feeding system, cooling devices, a counterbalance valve, etc. The reactor was made of high-strength corrosion-resistant stainless steel, which can sustain high pressure and temperature. The diameter of reactor and preheater were 20 mm and 26 mm, respectively. In addition, each section had a K-type thermocouple inserted for temperature control. The gas feeding system was controlled by means of several high-precision mass flow meters.

The pressure monitoring and controlling system was composed of a pressure sensor, a pressure gauge and a back pressure valve. The sensor was used to monitor the bed pressure drop and pressure stability of the whole experimental system was guaranteed by the back pressure valve and the pressure gauge. Meanwhile the exhaust section also included gas cooling and filtering devices to protect the back pressure valve.

The bed pressure drop (ΔP) was calculated as the difference between the measured pressured drop and distributor pressure drop. The distributor pressure drop is assumed to be:

$$\Delta P=\frac{\zeta \rho w^2}{2}$$

where ρ is gas density; w is gas velocity; ζ is correction coefficient. The ζ values at different temperature and pressure are shown in the Table 1.

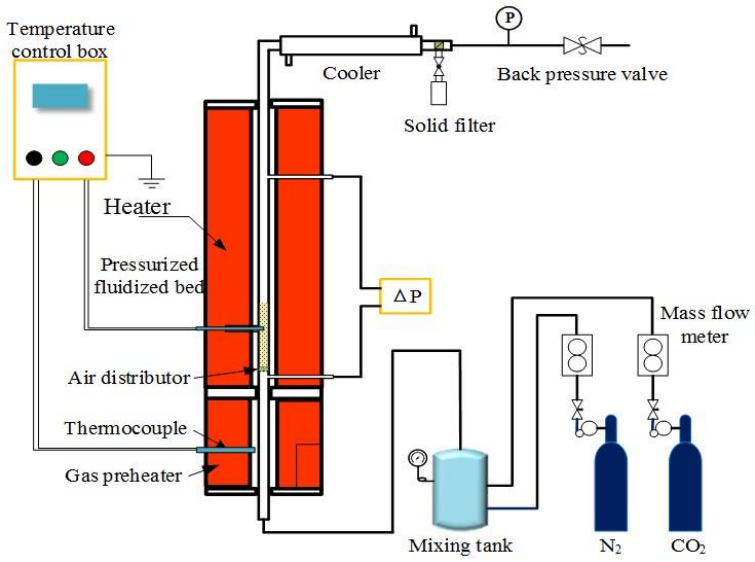

Fig. 1 Schematic diagram of the PFB system.

Table 1 The ζ values at different temperature and pressure

Pressure	ζ				
(MPa)	30°C	200°C	400°C	600°C	800°C

CO_2	0.1	6.64	4.20	3.82	3.80	3.52
	1.0	0.84	0.72	0.69	0.69	0.65
N_2	0.1	7.11	5.63	5.41	4.99	4.78
	1.0	1.02	0.81	0.85	0.81	0.78

2.1.2 Visualized pressurized fluidized bed

A “visible” and electrically heated fluidized bed combustor was used in this study. The schematic diagram of the experimental system is shown in Fig. 2. The two-dimensional (length: 200 mm, depth: 34 mm, height: 400 mm) PFB reactor was made of stainless steel, with a transparent quartz glass window (100 mm×200 mm) embedded into the front wall, which could provide information on flow behavior. A distributor consisting of four bubble caps with 0.416% open area (relative to the cross section of the bed) ensured uniform distribution of inlet gas. The preheating section and the reactor were heated by two 5 kW electrical heaters, respectively. The furnace temperature was controlled within 5˚C deviation by two PID controllers, which was verified by the measurement using a portable thermocouple. A high-speed CCD camera (Mikrotron GmbH，EoSens MC1362) was used to achieve real-time recording of the bubble behavior through the quartz window. The camera was focused on the center area of the reactor where the bubbles were most likely to appear.

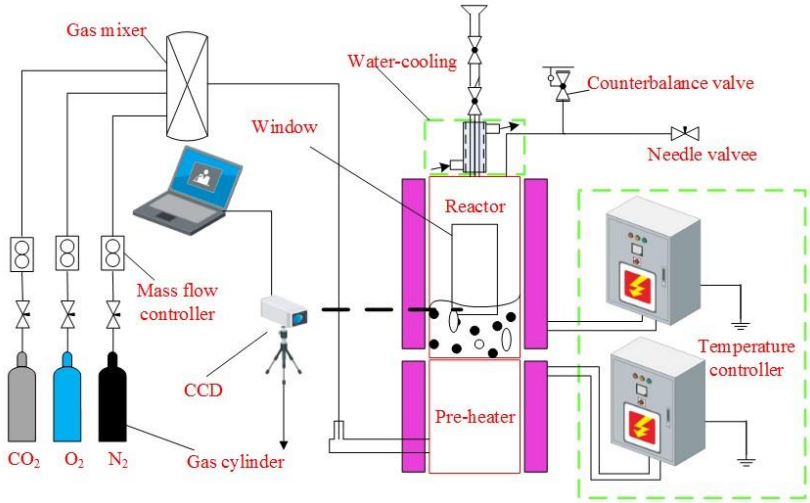

Fig. 2 Schematic diagram of visible pressurized fluidized bed system.

2.2 Materials

Quartz sands (size: 0.2-0.25 mm and 0.3-0.35 mm; density: 2560 kg/m^3) and iron powder (size: 0.1-0.15 mm; density: 7800 kg/m^3) were used as the bed material in the hot PFB (see Fig.1) with a static bed height of 150 mm. The 0.2-0.25 mm quartz sands was used to study the bubble behavior in the transparent PFB (see Fig.2). N_2 and CO_2 were used as the fluidized medium. The gas viscosity was calculated by the Chung method (Chung et al., 1988) and the results are shown in Fig. 3. The gas viscosity significantly increased with the increasing temperature, but did not change significantly with increasing pressure.

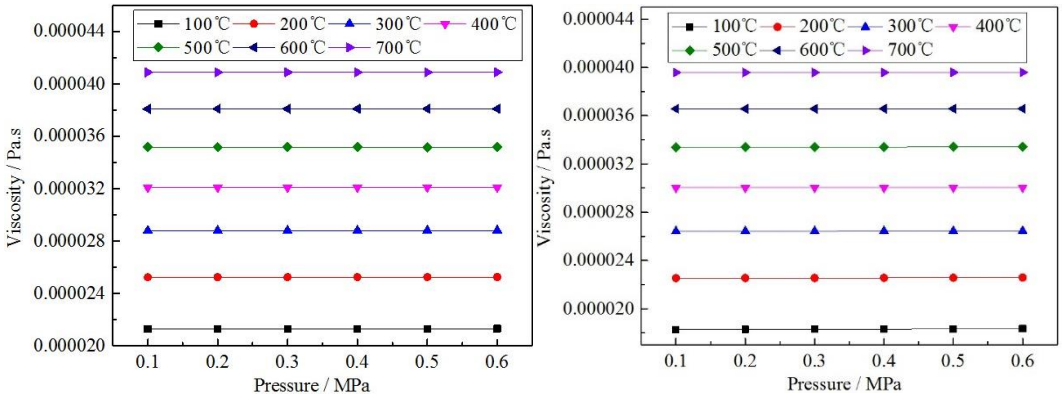

(a) N_2 (b) CO_2

Fig.3 The gas viscosity in different conditions.

2.3 Experimental procedure

About 150 mm high level of bed material was achieved by pouring the necessary amount of material into the fluidizing section of the column and then the reactor was heated to the desired temperature. Here, we set the system pressure to the target value by adjusting the back pressure valve, and fluidizing gas supply was increased to ensure that bed material fluidized vigorously. Then the gas flow rate was reduced slowly until the fluidized bed became a fixed bed. As the bed pressure drops during this process, bed pressures were recorded for each adjustment. In each test, a straight line was drawn from the origin through the series of bed pressure drop points until it crossed the horizontal line. It is widely accepted that u_{mf} can be taken as the velocity at the intersection point of the line. A detailed discussion on this method for the determination of u_{mf} can be found elsewhere (Ma et al., 2013).

The study of bubbling behavior was carried out in the system as shown in Fig. 2. When the system was stable at the desired pressure and temperature, the bubbling characteristics were recorded by the CCD through the quartz window, and then thousands of images under different conditions were collected on the bubble parameter information. Each test was repeated at least 3 times.

3. Results and Discussion

3.1 The minimum fluidization velocity

3.1.1 Gas atmosphere

The variations of u_{mf} versus system pressures for bed material of different particle sizes in atmosphere of N_2 or CO_2 are shown in Fig. 4. It is clear that with the increase of the pressure, the u_{mf} decreased, while the u_{mf} of large particles (0.85-1 mm) was significantly larger than that of small particles (0.3-0.35 mm). For the same particles experimented under the same pressure, the u_{mf} in N_2 atmosphere was slightly larger than that in a CO_2 atmosphere. This is caused by different physical properties of gas and particles. According to the Ergun formula (Ergun et al., 1952), the relationship between bed pressure drop (ΔP) and the gas velocity (u) in a fixed bed can be expressed as:

$$\frac{\Delta P}{H} = 150\frac{(1-\varepsilon)^2}{\varepsilon^3}\frac{\mu u}{d_v^2} + 1.75\frac{(1-\varepsilon)}{\varepsilon^3}\frac{\rho_f u^2}{d_v} \quad (2)$$

where ε is voidage of the bed; d_v is the equivalent volume diameter; H is the bed height; μ is the dynamic viscosity of gas; ρ_f is the gas density. When Reynolds number is small, the change in viscosity plays a major role. Inversely, with large Reynolds number, the effect of viscosity changes can normally be ignored. In this case formula (2) can be simplified as (Lasek et al., 2012):

$$Re_{mf} < 20, \qquad u_{mf} = \frac{d_p^2(\rho_p-\rho_f)g}{1650\mu} \quad (3)$$

$$Re_{mf} > 1000, \qquad u_{mf}^2 = \frac{d_p(\rho_p-\rho_f)g}{24.5\rho_f} \quad (4)$$

where d_p is the particle size; ρ_p is the particle density; g is the acceleration due to gravity. This research was carried out for low Reynolds number, thus the u_{mf} intensely depends on d_p^2. Furthermore, for the same particle, the u_{mf} is in proportion to $(\rho_p-\rho_f)/\mu$. Due to the different strength of the influence of density and viscosity value, the u_{mf} in CO_2 is

smaller than that in N_2. Considering the similar fluidization characteristics of CO_2 and N_2, N_2 is was employed as the fluidizing agent in the work described in section 3.1.2 to 3.2.4.

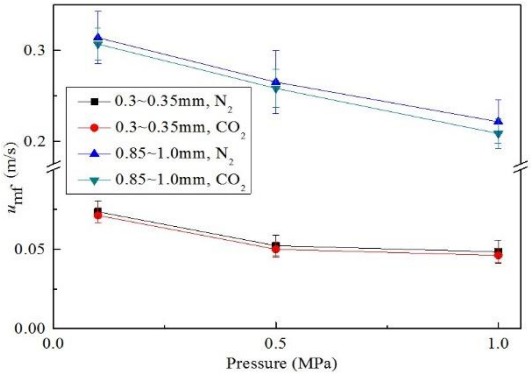

Fig.4 Variation of u_{mf} as a function of gas atmosphere, particle diameter and pressure.

3.1.2 Effects of operating temperature

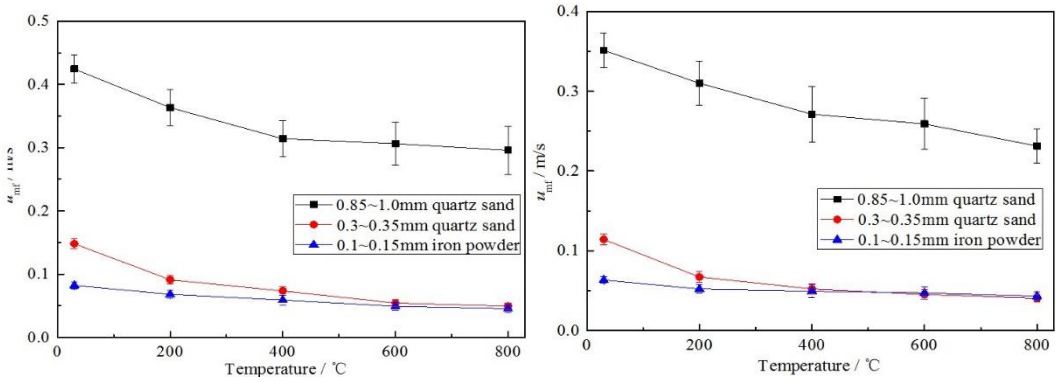

(a) 0.1 MPa (b) P=0.5 MPa

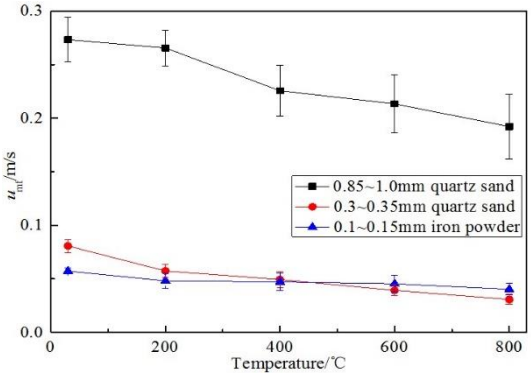

(c) P=1.0 MPa

Fig.5 The u_{mf} of quartz sand and iron powder in different temperature.

The u_{mf} of quartz sand (0.3-0.35 mm and 0.85-1 mm) and iron powder (0.1-0.15 mm) at different temperature are shown in Fig. 5. For both kinds of bed material with different particle size, u_{mf} decreased with increasing temperature, and this effect became larger for larger particle. This result is in agreement with the previous results (Goo et al., 2009; Subramani et al., 2007; Lin et al., 2002). When temperature rises, increased gas viscosity and pressure have opposing effects on value of u_{mf}. There is a viscous layer around smaller particles where gas viscosity is the most important (Formisani, 1998). It can be seen from Fig. 3 that the gas viscosity significantly increased with temperature, but that the size of this effect decreased. Therefore, the u_{mf} decreased with increased temperature. For larger particles, the fluidized region gradually became inertia-dominated, which means change of gas density cannot be ignored. Formisani (Formisani, 1998) indicated that larger particles were also more strongly influenced by particle sphericity and bed voidage. Here the gas viscosity and density, and bed voidage increased linearly with temperature. In conclusion, the way in which temperature affects u_{mf} is not only due to changing gas density and viscosity, but also altering interparticle filling characteristics.

3.1.3 Effects of operating pressure

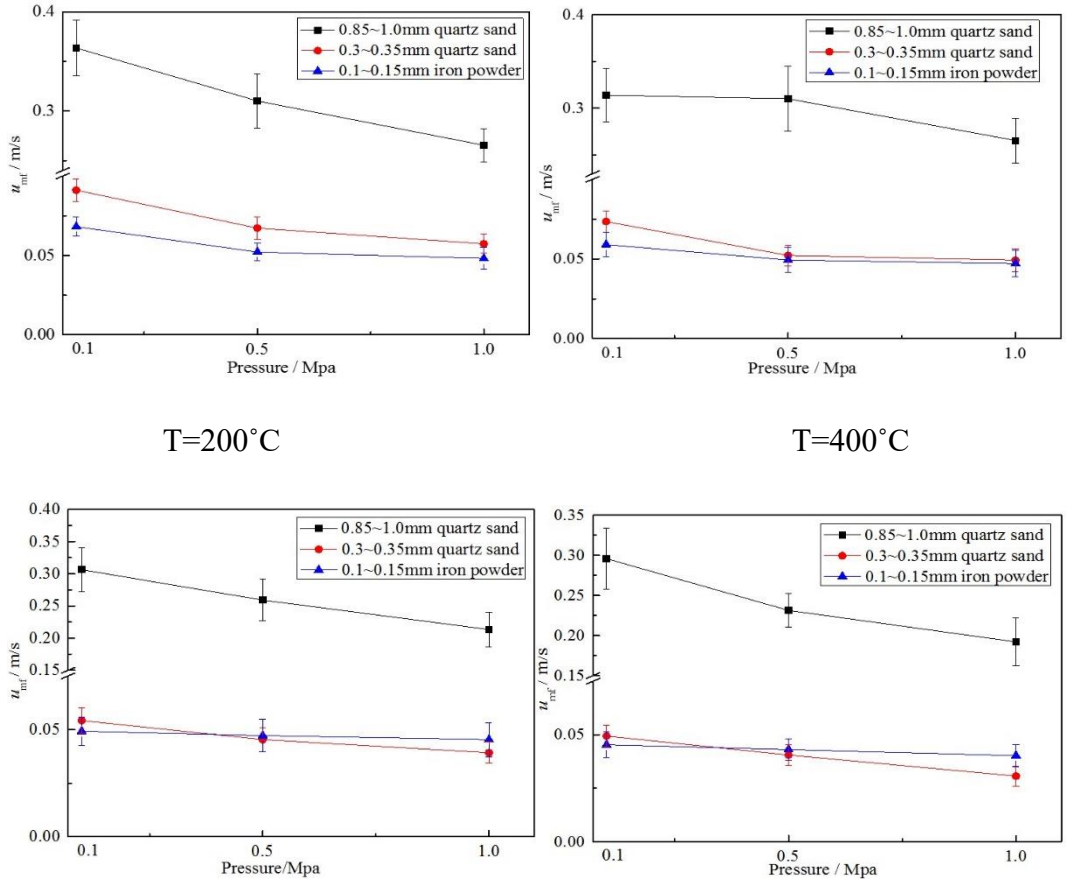

Fig. 6 Variation of u_{mf} as a function of pressure.

The u_{mf} of quartz sand and iron powder under different pressures is shown in Fig. 6. The u_{mf} clearly decreased as the pressure increase and the decrease grew bigger for the larger bed material particles. Interestingly, the u_{mf} of iron powder (0.1-0.15 mm) is almost constant under different pressures. The gas around smaller particles was nearly laminar flow, based on formula (3). Since the iron powder density is much larger than that of N_2, (ρ_p-ρ_f) is almost constant. Therefore the u_{mf} was decided by gas viscosity which was is barely affected by pressure (see Fig. 3), ensuring that the u_{mf} of iron powder (0.1-0.15 mm) did not change with pressure. As the particle size increased, the

flow became gradually turbulent. According to formula (4), the u_{mf} is proportional to $d_p(\rho_p-\rho_f)$ and inversely proportional to ρ_f. Gas density is positively correlated with pressure, so the u_{mf} decreased with as pressure increased and the decrease was influenced by particle size. Consequently, the u_{mf} is controlled by gas viscosity for the smaller particles under various pressures. For the larger bed material, u_{mf} is mainly decided by gas density under different pressures.

3.1.4 Formula fitting

In this work, the form of $Re_{mf} = [C_1^2+C_2Ar\ ]^{0.5}-C_1$ was adopted to fit the formula for calculating u_{mf}, which was derived from Ergun equation and had been used extensively (Kunii, 1991). The experimental data and the fitted curve is shown in Fig. 7, in which C_1 and C_2 are 31.56 and 0.043, respectively. The equation obtained by fitting the values is shown below:

$$u_{mf} = \mu\left[\sqrt{31.56^2 + 0.043Ar} - 31.56\right]/d_p\rho_g \quad (5)$$

The relative error between fitted values and experiment value is calculated to be less than 15%, ranging from 1.37% to 14.79%, which proves the reliability of the equation. The u_{mf} is a basic parameter for CFB in design and operation. Therefore, it is necessary to emphasize that all empirical equations including (5) have a specific scope of application, and there can be severe errors when the application conditions exceed the appropriate experimental range.

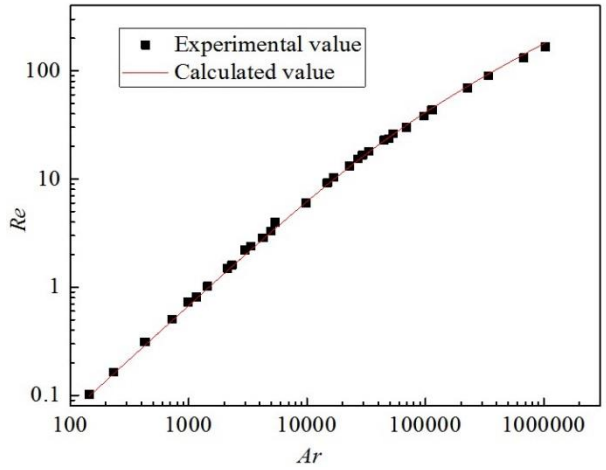

Fig. 7 Comparison between calculated experimental results.

Table 2 summarizes some empirical formulas used to predict the u_{mf}. Calculation of u_{mf} with different equations at 200 ˚C and 800 ˚C are shown in Fig. 8. Formula (2) and (10) were based on the mechanical model of a single particle, which only considers gravity, buoyancy and drag force on the particle. Ignoring the role of frictional force may therefore cause large errors when it is great enough. Formula (1) and (3)-(9) are derived from Ergun equation and static balance, assuming the bed voidage is constant. The experimental conditions of Formula (6) was at high temperature, and the others were carried out at ambient temperature. Formula (7) was used for ambient temperature and high pressure conditions. However, variation of voidage when present at high temperature and pressure may result in deviation. It should be pointed out that the formula (9) is the closest to the result of present work. This may be because their experimental conditions were closer to those of this paper.

Table 2 The empirical formula used to predict u_{mf}

NO.	Author	Correlation	Conditions
1	Wen and Yu	$Re_{mf} = [33.7^2+0.0408Ar]^{0.5}-33.7$	Various particles, 0.04~20 mm, ambient temperature, $0.001 < Re_{mf} < 4000$

2	Doichev and Akhmakov	$Re_{mf} = 0.00108Ar^{0.947}$	Glass beads, 0.09~2.2 mm, ambient temperature, ρ_p=2650 kg/m^3
3	Richardson and Jeronimo	$Re_{mf} = [25.7^2+0.0365Ar]^{0.5}-25.7$	——
4	Babu, et al	$Re_{mf} = [25.25^2+0.0651Ar]^{0.5}-25.25$	0.05~2.87 mm, ambient temperature, 0.02< Re_{mf} < 170
5	Saxena and Vogel	$Re_{mf} = [25.28^2+0.0571Ar]^{0.5}-25.28$	0.088~1.41 mm, ambient temperature, 6< Re_{mf} <102, ρ_p = 3190 kg/m^3
6	Zheng, et al	$Re_{mf} = [18.75^2+0.0313Ar]^{0.5}-18.75$	Glass beads and quartz sand, 20~700 ˚C
7	Chitester	$Re_{mf} = [28.7^2+0.0494Ar]^{0.5}-28.7$	Coal, char and Ballotini, 88~374 μm, ambient temperature, high pressure
8	Grace	$Re_{mf} = [27.2^2+0.0408Ar]^{0.5}-33.7$	——
9	Thonglimp, et al	$Re_{mf} = [31.6^2+0.0425Ar]^{0.5}-31.6$	Aluminium oxide, Glass beads and steel ball, 112~2125 μm, 1.6~7.4 g/cm^3
10	Barbosa, et al	$Re_{mf} = 0.0019Ar^{0.87}$	——

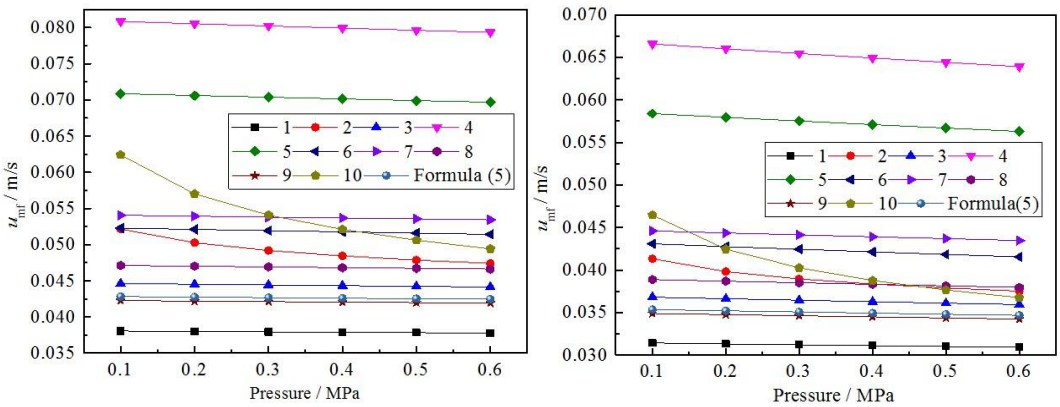

（a）200 ˚C　　（b）800 ˚C

Fig. 8 Comparison among different and empirical formula results of $u_{mf.}$

3.2 Bubble characteristics

3.2.1 The minimum bubbling velocity (u_{mb})

The u_{mb} of quartz sand (0.2-0.25 mm) for different temperature and pressure are plotted in Fig. 9. It is clear that the u_{mb} significantly decreased as the temperature and pressure increased. This is in agreement with the results of Li et al. (2013), who carried out experiment at atmospheric temperature. Li et al. found that as the pressure increased,

the u_{mf} decreased and the value of u_{mb}/u_{mf} remained at 1 for Geldart B particles which are used here. When the gas velocity exceeds u_{mf}, the "excess gas" increases local voidage and bubbles formation. Therefore, the value of u_{mb} has a positive correlation with u_{mf}. In this study, the gas flow around the quartz sand particles was for laminar conditions, which was mainly affected by two parameters: (1) Gas viscosity. The gas viscosity decreases slightly with the increase of pressure, but is not sensitive to pressure. By contrast, it increases remarkably with the elevation of temperature. (2) Gas density. The gas density increases with increasing pressure decreases with increasing temperature. According to the formula (3), higher pressure will cause a decrease the u_{mf} by enhancing the gas density. For Geldart B particles, the umf and umb are almost equal. So the higher pressure will cause a decrease the u_{mb}. Although the gas density decreased with increasing temperature, a slight drop of gas density has little effect on the density difference between gas and solid particle. Therefore, the u_{mb} decreases with the increase of temperature due to the combined effects of density and viscosity.

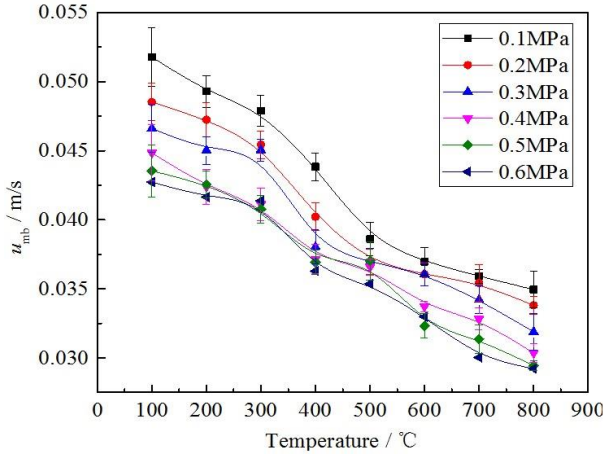

Fig. 9 Variation of minimum bubbling velocity as a function of temperature/pressure.

3.2.2 Bubble behavior

Typical images captured for studying bubble behavior with different fluidization number ($w=u/u_{mf}$) at 800 ˚C and 0.1MPa are displayed in Fig. 10. The whole process included bubble appearance, bubble escape from the bed, break-up and the tail vortex entering into the freeboard. From the recorded image, it could be seen that as the *w* increased, the diameter of bubble, the volume and height of tail vortex all increased remarkably. Additionally, bubbles tended to merge and bubble shape became more irregular. The reason was that the velocity of bubble and "excess gas" increased with the larger fluidization number, leading to larger bubbles and more kinetic energy of tail vortex. When the bubbles are rising through the bed, a low-pressure area is formed in the lower part of bubbles, causing some particles (the so called bubble vortex) to follow the rising bubble. In a multi-bubble system, the rising bubbles may merge into a larger bubble, or break into two small bubbles, and their shape will change consequently (Jin et al., 1991). At smaller fluidization numbers, there was less interference between bubbles and their shape was close to being spherical. With the increase of the fluidization number, bubbles gradually started to transform and become extremely irregular due to dramatic turbulence in the bed, then the capture of the bubble size from the visual images became very difficult. In order to eliminate the influence of the interaction between bubbles, *w* was set to 1.5-2.5 and the effect of these parameters on bubble behavior are analyzed below.

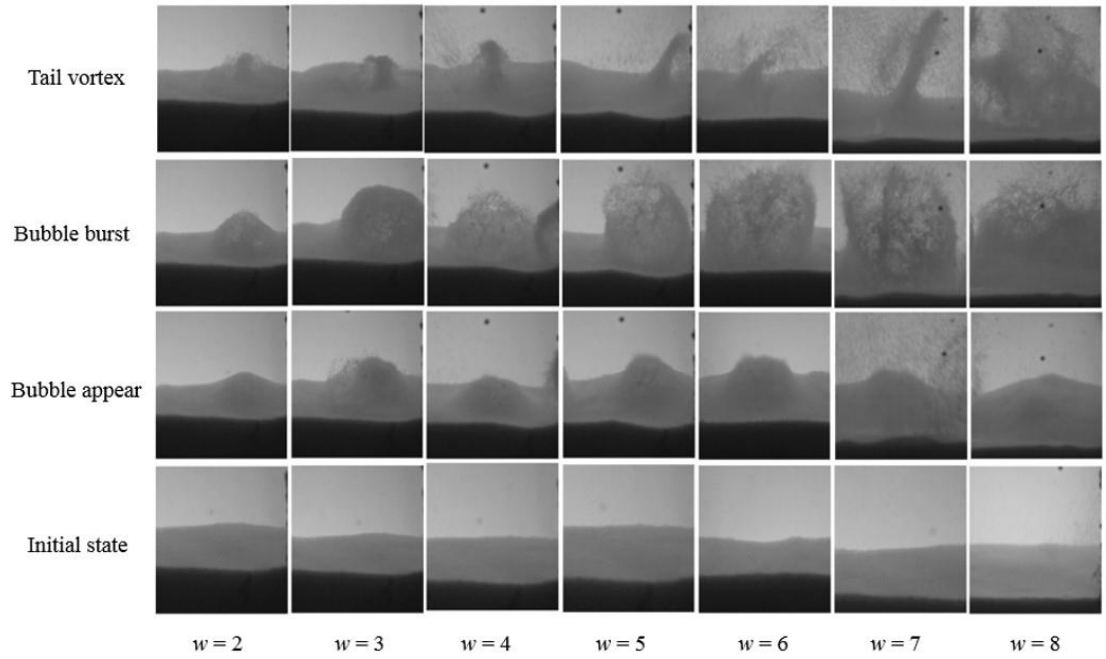

Fig. 10 The evolution process of bubbles at different fluidization number (800 ˚C, 0.1MPa).

3.2.3 Bubble diameter

Variation of the average bubble diameter (D_b) with different fluidization numbers, temperature and pressure are shown in Fig. 11. It is clear that with the increase of fluidization number, the bubble diameter increased almost linearly, while the bubble diameter decreased remarkably with the increase of temperature and pressure. Rowe et al. (Rowe et al., 1984) conducted X-ray observation of gas-fluidized beds under different pressure at room temperature, and observed very similar experimental phenomenon. However, Hoffmann et al. (1986), who conducted tests by using porous Al_2O_3 (mean grain size: 0.45 mm, density: 1417kg/m^3) as the bed material; with the value of u-u_{mf} set as 2.8 cm/s and 3.9 cm/s, found that bubble size first increased and then decreased as pressure went up. This may be caused by the fixed value of u-u_{mf},

which enhanced the fluidization number at high pressure. Li et al. (2013) carried out experimental investigations (bed material: quartz sands) in different pressures with two values of u-u_{mf}. The results showed that when u-u_{mf}=0.5 cm/s, the variation of bubble diameter with pressure was consistent with this work, while it agreed with Hoffmann et al. (1986) when u-u_{mf}=0.2 cm/s. Therefore, various values of u-u_{mf} may affect the changing trend of bubble size. In addition, elevated pressure can result in break-up of bubbles which may be another reason for the decrease in bubble size (Li et al., 2013).

3.2.4 Bubble frequency

In this work, bubble frequency (f) represents the occurrence of the average number of bubbles on the bed surface per unit time. Here, only a fluidization number of 1.5 was studied because at higher velocity, the bubble coalescence occurs and large measurement error will be generated. Each test condition was recorded by CCD at 300 frames/s for 3 s. The index for bubble frequency was determined by counting the number of bubbles escaped from the bed by processing the images. Bubble frequency for different fluidization number, temperature and pressure are displayed in Fig. 12. In this work, bubble frequency increased with the increase of fluidization number, because the higher fluidization number means more “excess gas” passing through bed per unit time, which forms more bubbles. It could also be shown that the bubble frequency slightly decreased with the increase of temperature and pressure. As described in 3.1.2 and 3.1.3, u_{mf} decreased with the increase of temperature and pressure, so the same fluidization number resulted in less “excess gas” to form bubbles.

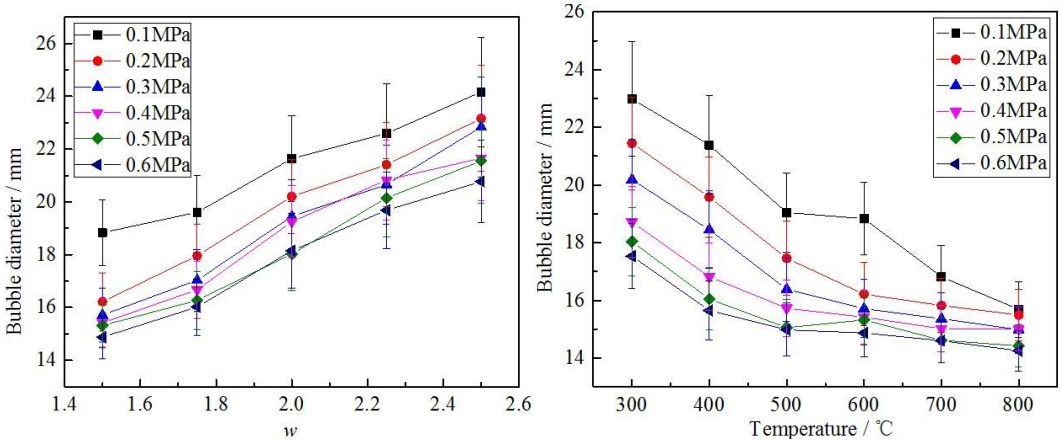

(a) *w* (600 ˚C) (b) Temperature (*w*=1.5)

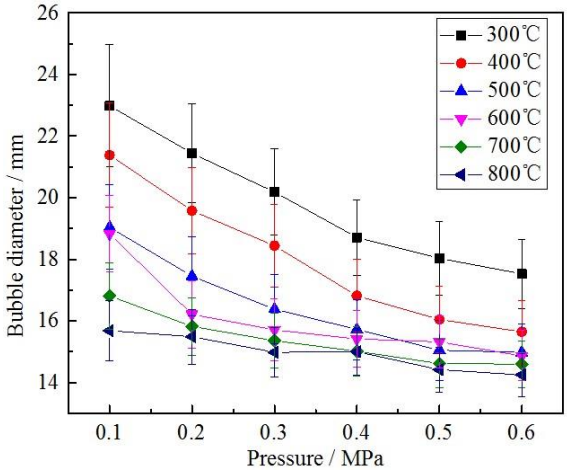

(c) Pressure (*w*=1.5)

Fig. 11 Average diameters of bubble with different fluidization number, temperature and pressure.

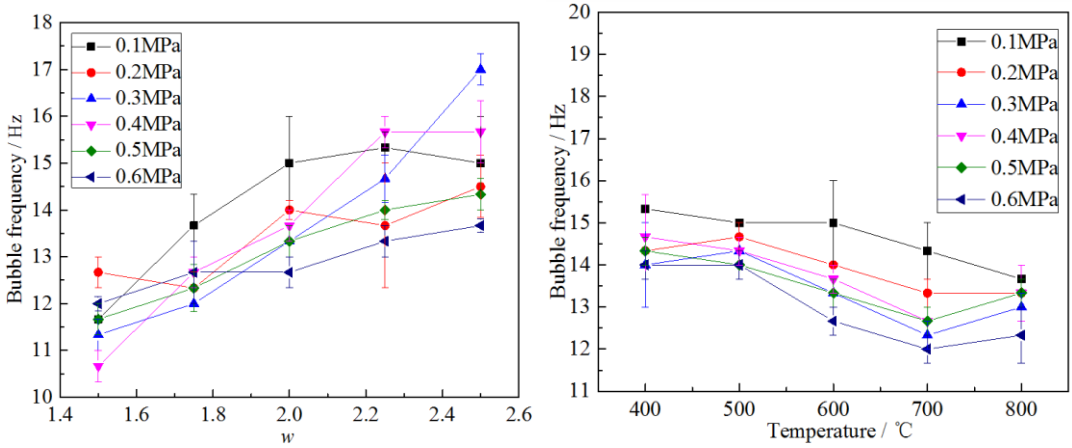

(a) *w* (600 ˚C) (b) Temperature (*w*=1.5)

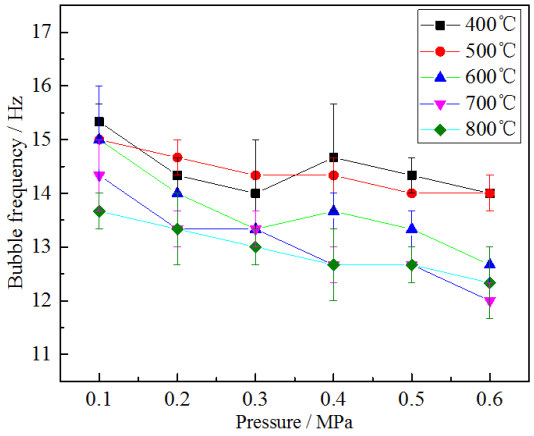

(c) Pressure (*w*=1.5)

Fig. 12 Variation of bubble frequency as a function of fluidized number, temperature and pressure.

4 Conclusion

The goals of this study are to obtain the flow characteristics of fluidized bed under high temperature and high pressure, representing the pressurized oxy-fuel fluidized bed condition. The minimum fluidization velocity, minimum bubbling velocity, bubble morphology, bubble diameter and bubble frequency were studied in detail. The following conclusions can be drawn as follows:

(1) The minimum fluidization velocity decreases with rising pressure and temperature, and this effect increases with larger particle.

(2) Based on experimental results, the formula for calculating the minimum fluidization velocity of pressurized fluidized bed was fitted to the data, and the relative error was within 15%.

(3) The minimum bubbling velocity decreases with increasing temperature and

pressure.

(4) The diameter of bubbles decreases with the increase of temperature and pressure, and bubble frequency goes up with increased fluidization number, but decreases with an increase of temperature and pressure.

Acknowledgments

This work was financially supported by the National Natural Science Foundation of China (NO. 51776039).

References

Basu P, Fraser S A. Circulating fluidized bed boilers design and operations [M]. Boston：Butterworth-Heinemann, 1991: 24.

Buhre, B.J.P., Elliott, L.K., Sheng, C.D., Gupta, R.P., Wall, T.F., 2005. Oxy-fuel combustion technology for coal-fired power generation. Prog. Energy Combust. Sci. 31, 283-307. doi: 10.1016/j.pecs.2005.07.001.

Benelli, G., Cumbo, D., Gazzino, M. Pressurized oxy-combustion of coal with flue gas recirculation: pilot scale demonstration. Power Gen Europe conference and exhibition, Milan, Italy.

Busciglio, A., Vella, G., Micale, G., Rizzuti, L., 2008. Analysis of the bubbling behavior of 2D gas fluidized beds. Part I. Digital Image Analysis Technique. Chem. Eng. J. 140, 398-413. doi: 10.1016/j.cej.2007.11.015.

Chitester, D., Kornosky, R., Fan, L., Danko, J., 1984. Characteristics of fluidization at high pressure. Chem. Eng. Sci. 39, 253-261. doi: 10.1016/0009-2509(84)80025-1.

Caicedo, G.R., Marque´s, J.J.P., Ruis, M.G., Soler, J.G., 2003. A study on the behaviour of bubbles of a 2D gas–solid fluidized bed using digital image analysis. Chem. Eng. Process. 42, 9-14. doi: 10.1016/S0255-2701(02)00039-9.

Chung, T.H., Ajlan, M., Lee, L.L., Starling, K.E., 1988. Generalized multiparameter correlation for nonpolar and polar fluid transport properties. Ind. Eng. Chem. Res. 27, 671-679. doi: 10.1021/ie00076a024.

Duan, Y., Duan, L., Anthony, E.J., Zhao, C., 2017. Nitrogen and sulfur conversion during pressurized pyrolysis under CO_2 atmosphere in fluidized bed. Fuel 189, 98-106. doi: 10.1016/j.fuel.2016.10.080.

Ergun S., 1952. Fluid flow through packed columns. Chem. Eng. Prog. 48, 89-94.

Formisani, B., Girimonte, R., Mancuso, L., 1998. Analysis of the fluidization process of particle beds at high temperature. Chem. Eng. Sci. 53, 951-961. doi: 10.1016/S0009-2509(97)00370-9.

Girimonte, R., Formisani, B., 2009. The minimum bubbling velocity of fluidized beds operating at high temperature. Powder Technol. 189, 74-81. doi: 10.1016/j.powtec.2008.06.006.

Goo, J., Seo, M., Kim, S., Song, B., 2009. Effects of temperature and particle size on minimum fluidization and transport velocities in a dual fluidized bed. Proceedings of the 20th International Conference on Fluidized Bed Combustion, Xi’an, China.

Grace J., 1983. Hydrodynamics of Liquid Drops in Immiscible Liquids. Handbook of Fluids in Motion, 38.

Hansen, J., Johnson, D., Lacis, A., Lebedeff, S., Lee, P., Rind, D., Russell, G., 1981. Climate impact of increasing atmospheric carbon dioxide. Science 213, 957-66. doi: 10.1126/science.213.4511.957.

Hoffmann, A.C., Yates. J.G., 1986. Experimental Observations of fluidized beds at elevated pressures. Chem. Eng. Commun. 41, 133-149. doi: 10.1080/00986448608911716.

Jin, Y., Zhu, J., Wang, Z.W., Yu, Z.Q., 1991. Fluidization engineering principles. Beijing: Tsinghua University Press, 21-23.

King, D.F., Harrison, D., 1982. Dense phase of a fluidized bed at elevated pressures. Transactions of the Institution of Chemical Engineers 60, 26-30.

Kunii, D., Levenspiel, O., 1991. Fluidization engineering. Butterworth-Heinemann.

Lasek, J.A., Janusz, M., Zuwała, J., Głód, K., Lluk, A., 2013. Oxy-fuel combustion of selected solid fuels under atmospheric and elevated pressures. Energy 62, 105-112. doi: 10.1016/j.energy.2013.04.079.

Lasek, J.A., Głód, K., Janusz, M., Kazalski, K., Zuwała, J., 2012. Pressurized oxy-fuel combustion: A study of selected parameters. Energy Fuels 26, 6492-6500. doi: 10.1021/ef201677f.

Lei, M., Huang, X., Wang, C., Yan, W., Wang, S., 2016. Investigation on SO_2, NO and NO_2 release characteristics of Datong bituminous coal during pressurized oxy-fuel combustion. J. Therm. Anal. Calorim. 126, 1067-1075. doi: 10.1007/s10973-016-5652-y.

Li, H., Yan, W., Wei, W., Wang, C., 2013. Characteristics of fluidisation behaviour in a pressurised bubbling fluidised bed. Can. J. Chem. Eng. 91, 760-769. doi: 10.1002/cjce.21723.

Lin, C., Wey, M., You, S., 2002. The effect of particle size distribution on minimum fluidization velocity at high temperatures. Powder Technol. 126, 297-301. doi: 10.1016/S0032-5910(02)00074-8.

Li, H.Y., 2013. Research on Fluid Dynamic and Radiative Heat Transfer in Pressurized Oxygen-enriched Fluidized Bed Combustion (D). Beijing: North China Electric Power University. (In Chinese)

Ma, J., Chen, X., Liu, D., 2013. Minimum fluidization velocity of particles with wide size distribution at high temperatures. Powder Technol. 235, 271-278. doi: 10.1016/j.powtec.2012.10.016.

Movahedirad, S., Dehkordi. A.M., Banaei, M., Deen, N.G., Annaland, M.V.S., Kuipers, J.A.M., 2012. Bubble Size Distribution in Two-Dimensional Gas-Solid Fluidized Beds. Ind. Eng. Chem. Res. 51, 6571-6579. doi: 10.1021/ie300027p.

Rowe, P.N., Foscolo, P.U., Hoffman, A.C., Yates, J.G., 1984. X-ray observation of gas-fluidized beds under pressure. Engineering Foundation 4, 53-60.

Shaddix, C.R., 2012. Coal combustion, gasification, and beyond: Developing new technologies for a changing world. Combust. Flame 159, 3003-3006. doi: 10.1016/j.combustflame.2012.07.013.

Sidorenko, I., Rhodes, M.J., 2004. Influence of pressure on fluidization properties.

Powder Technol. 141, 137-154. doi: 10.1016/j.powtec.2004.02.019.

Sobreiro, L.E., Monteiro, J.L., 1982. The effect of pressure on fluidized bed behavior. Powder Technol. 33, 95-100. doi: 10.1016/0032-5910(82)85043-2.

Saxena, S.C., Vogel, G.J., 1977. The measurement of incipient fluidization velocities in a bed of coarse dolomite at temperature and pressure. Transaction of the Institution of Chemical Engineers 55, 184-189.

Subramani, H.J., Balaiyya, M.B.M., Miranda, L.R., 2007. Minimum fluidization velocity at elevated temperatures for Geldart's group-b powders. Exp. Therm. Fluid Sci. 32, 166-173. doi: 10.1016/j.expthermflusci. 2007.03.003.

Shen, L., Johnsson, F., Bo, L., 2004. Digital image analysis of hydrodynamics two-dimensional bubbling fluidized beds. Chem. Eng. Sci. 59, 2607-2617. doi: 10.1016/j.ces.2004.01.063.

Thonglimp V., Hiquily N., Laguerie C., 1984. Vitesse minimale de fluidisation et expansion des couches fluidisées par un gaz. Powder Technology 38, 233-253. doi: 10.1016/0032-5910(84)85006-8.

Yang W., Chitester D., Kornosky R., Keairns D., 2010. A generalized methodology for estimating minimum fluidization velocity at elevated pressure and temperature. Aiche Journal 31, 1086-1092. doi: 10.1002/aic.690310706.

Figure captions

Fig. 1 Schematic diagram of the PFB system.

Fig. 2 Schematic diagram of visible pressurized fluidized bed system.

Fig.3 The gas viscosity in different conditions.

Fig.4 Variation of u_{mf} as a function of gas atmosphere.

Fig.5 The u_{mf} of quartz sand and iron powder in different temperature.

Fig. 6 Variation of u_{mf} as a function of pressure.

Fig. 7 Comparison between calculated experimental results.

Fig. 8 Comparison among different and empirical formula results of $u_{mf.}$

Fig. 9 Variation of minimum bubbling velocity as a function of temperature/pressure.

Fig. 10 The evolution process of bubbles at different fluidization number.

Fig. 11 Average diameters of bubble with different fluidization number, temperature and pressure.

Fig. 12 Variation of bubble frequency as a function of fluidized number, temperature and pressure.

Table 1

The ζ values at different temperature and pressure

	Pressure (MPa)	ζ				
		30°C	200°C	400°C	600°C	800°C
CO_2	0.1	6.64	4.20	3.82	3.80	3.52
	1.0	0.84	0.72	0.69	0.69	0.65
N_2	0.1	7.11	5.63	5.41	4.99	4.78
	1.0	1.02	0.81	0.85	0.81	0.78

Table 2

The empirical formula used to predict u_{mf}

NO.	Author	Correlation	Conditions
1	Wen and Yu	$Re_{mf} = [33.7^2+0.0408Ar]^{0.5}-33.7$	Various particles, 0.04~20 mm, ambient temperature, $0.001 < Re_{mf} < 4000$
2	Doichev and Akhmakov	$Re_{mf} = 0.00108Ar^{0.947}$	Glass beads, 0.09~2.2 mm, ambient temperature, ρ_p=2650 kg/m^3
3	Richardson and Jeronimo	$Re_{mf} = [25.7^2+0.0365Ar]^{0.5}-25.7$	——
4	Babu, et al	$Re_{mf} = [25.25^2+0.0651Ar]^{0.5}-25.25$	0.05~2.87 mm, ambient temperature, $0.02< Re_{mf} < 170$
5	Saxena and Vogel	$Re_{mf} = [25.28^2+0.0571Ar]^{0.5}-25.28$	0.088~1.41 mm, ambient temperature, $6< Re_{mf} <102$, ρ_p = 3190 kg/m^3
6	Zheng, et al	$Re_{mf} = [18.75^2+0.0313Ar]^{0.5}-18.75$	Glass beads and quartz sand, 20~700 ˚C
7	Chitester	$Re_{mf} = [28.7^2+0.0494Ar]^{0.5}-28.7$	——
8	Grace	$Re_{mf} = [27.2^2+0.0408Ar]^{0.5}-33.7$	——
9	Thonglimp, et al	$Re_{mf} = [31.6^2+0.0425Ar]^{0.5}-31.6$	Aluminium oxide, Glass beads and steel ball, 112~2125 μm, 1.6~7.4 g/cm^3
10	Barbosa, et al	$Re_{mf} = 0.0019Ar^{0.87}$	——